Forces in Mechanics 14 (2024) 100251

Contents lists available at ScienceDirect

Forces in Mechanics

journal homepage: www.sciencedirect.com/journal/forces-in-mechanics

Design aspects of a CMC coating-like system for hot surfaces of aero engine components

Giacomo Canale [a], Felice Rubino [b,*], Roberto Citarella [c]

[a] University of Derby, Markeaton Street, Derby DE22 3AW, UK
[b] Department of Civil and Mechanical Engineering, University of Cassino and Southern Lazio, Cassino, FR, Italy
[c] Department of Industrial Engineering, University of Salerno, Fisciano, SA, Italy

ARTICLE INFO

Keywords:
Creep calibration
Coating stress analysis procedure
Thickness optimization
Thermo-mechanical analysis

ABSTRACT

Ceramic Matrix Composite (CMC) is an emerging material system that can be a game changer in the aerospace industry, both civil and military. CMCs components are, in fact, lighter and less prone to fatigue failure in a high temperature environment. However, at high temperatures, the diffusion of oxygen and water vapour inside the CMC can have detrimental effects. Therefore, the presence of protective coating is necessary to extend the life of CMC components. In the present work, a three-layers coating, consisting of a silicon bond (BND), adhesively bonded to the CMC, an Environment Barrier Coating (EBC) and a softer layer 3 (LAY3), is investigated for a CMC component. An aero-engine high pressure turbine seal segment was considered. Two design aspects are covered: (i) creep law is determined and calibrated in environment Abaqus from the experimental data of each coating layer available in the open literature, to provide a suitable instrument for the creep relaxation analyses of hot components; (ii) thickness sensitivity study of each layer of the coating is conducted to minimise the interface stresses of coating with substrate in order to mitigate cracking and removal/spalling phenomena when exposed to temperature gradients and to increase their service life. These two different aspects are combined together to predict the coating stress field as a function of service time.

1. Introduction

Silicon Carbides (Sic/Sic) Ceramic Matrix Composites (CMC) could be a game changer in the aero-engine industry [1]. Main advantages are their strength at high temperatures [2,3] and their weight advantage compared to traditional materials conventionally used for a Turbine Sub-system component such like nickel super alloys [4], including their single crystal design variant [5]. CMCs have one third of the density of their metallic counterpart and offer superior structural performance at elevated temperatures. Furthermore, the decay in strength and stiffness is much less pronounced with respect to the metallic nickel alloys for temperature even 200°C higher than their service temperature [6]. Therefore, CMCs represent a promising alternative in aero-engine High Pressure Turbine System allowing to reach higher turbine operative temperatures, which would improve the thermal efficiency of the turbine component and the propulsive efficiency of the engine, contribute positively to the reduction of NOx emissions [7]. However, one of the main challenges for this type of CMC is the silica formation and evaporation driven by oxidation [8,9]. For this reason, a protective coating is necessary [10–13]. The designed coatings will act as a thermal and environmental barrier against the high temperature oxidation environment [14,15]. These coatings are commonly manufactured by means of thermal spray techniques, such as high velocity oxygen fuel (HVOF), atmospheric or low-pressure plasma spraying, to mention but a few [16–23].

The sealing coating is composed by three layers (Fig. 1). They are, in order from the interface with the substrate: (i) the silicon bond layer (BND), which allows the bonding between the CMC substrate and the coating and mitigates the mismatch in the thermal expansion coefficients of them; (ii) the Environmental Barrier Coating (EBC) which exerts the actual protective function against the working environment; (iii) the external sacrificial softer layer (often defined as abradable [26]) needed to control the tip clearances for the aero engine performance improvement [10,24–26]. Both sacrificial layer (hereinafter indicates as LAY3) and EBC are made of Ytterbium disilicate, $Yb_2Si_2O_7$. The and the EBC differ each other for the percentage of porosity existing in both coating layers [26,27], as visible in Fig. 1.

The porosity, desired for LAY3 [28], while unwanted in the EBC, is

* Corresponding author.
E-mail address: f.rubino@unisa.it (F. Rubino).

https://doi.org/10.1016/j.finmec.2023.100251
Received 6 December 2023; Received in revised form 21 December 2023; Accepted 22 December 2023
Available online 5 January 2024

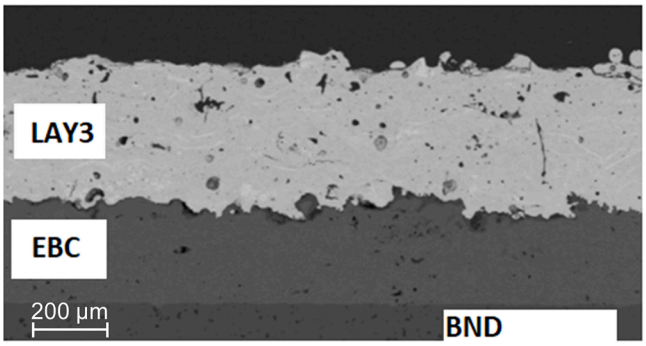

Fig. 1. A SEM image of the 3 layers of the coating system investigated in this work [10].

crucial to limit oxygen and water vapour diffusion and for the structural integrity of the coating. The bond coat, beside promoting the bonding between two different materials, also acts as a "reservoir" to retain oxidisers before they react with the underlying CMC substrate providing a further protection.

Coating spraying process, in fact, induces a residual stress [29] that tends to be modified with the heat treatment and with the in-service conditions (both mechanical and thermal loads). Accurate predictions of deformation and potential stress relaxation of the coating during the flight cycle and more during its in-service life are, therefore of paramount importance. Creep data have been measured and made available in the published literature [30,31]. In the first part of the paper, a creep law model has been coded by using an Abaqus Sub-routine and the calibration of creep law parameters has been conducted by using the creep data available in the published literature for the material systems (BND and EBC) [30,31] and following the procedures reported in the open literature [32,33]. The second part of the work deals with the optimisation of the thickness of each coating layer subjected to thermal gradients [34]. To author's best knowledge, this aspect is relatively unexplored in the open literature for CMC coating systems. The aim of the optimization is to find an optimal configuration of the coating to minimise the interface stresses between the layers of the coating and between the coating and the CMC substrate, responsible for cracking and coating loss in service. Minimising these stresses would increase the chances of a longer in-service-life. Silica depletion [35] and Thermally Grown Oxide (TGO) [36] (Thermally-Grown-Oxide) at the bond interface are not considered at this stage but could be included as a part of future work.

2. Experimental creep data conversion to Abaqus

Experimental data of BND have been produced at different temperatures for a stress point of 8.3 MPa. Details of the creep experiments are given in [30,31]. All creep tests were performed in air by using a 4-point bending fixture. It is here remarked that the results given by this kind of test is for qualitative understanding and general trend only. The raw data are presented in Fig. 2a. The experimental data of the EBC coating for a stress point of 15.8 MPa are shown in Fig. 2b.

In Fig. 2a, isothermal 4-point flexure creep data of the silicon bond (BND) are shown for three different temperatures, at which the component layer is potentially supposed to operate at different flight conditions. Two phases of the creep inelastic strain are clearly visible: primary creep and secondary creep. The biggest contribution to the creep strain is given by the primary creep. It is important to remark that consistent behavior is observed at the three temperature regimes and no relevant inelastic creep strain has been measured in the experiments performed below 1273 K. The stress level chosen to produce the experimental data is 8.3 MPa. This is a potential BND stress value in

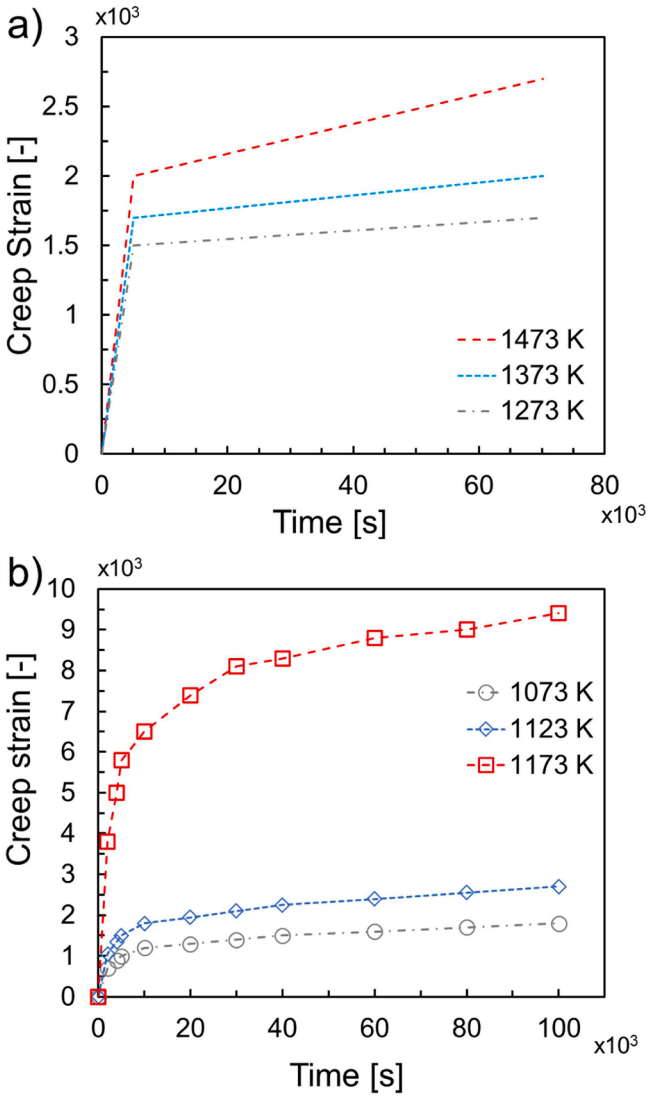

Fig. 2. (a) silicon BND raw creep data (experimental) at different temperatures; (b) EBC raw creep data (experimental) at different temperatures

cruise (not in transient heating up or cool down phases). The condition at which the BND will spend more operative time and therefore the one more likely to cause creep. In Fig. 2b, experimental data of plasma sprayed $YbSi_2O_7$ EBC are given. The data are reported for three different temperatures regimes and for a stress of 15.8 MPa. Same comments written for the BND concerning stress and temperatures, primary and secondary creep, also apply for the EBC. Experimental data has been recorded every 0.2 s.

Concerning the silicon bond, a power law time equation [37] has been initially implemented in Abaqus by using a user sub-routine. The power law initially used is given in Eqn.1.

$$\epsilon_{cr} = \frac{c_1}{c_3+1}\sigma^{c_2} t^{1+c_3} e^{\frac{-c_4}{T}} + c_5 \sigma^{c_6} e^{\frac{-c_7}{T}} t \tag{1}$$

Where, ε_{cr} is the creep strain, calculated with the analytical approach of adding primary and secondary components, σ is the Von Mises Stress, T is the temperature expressed in Kelvin, t is the time in seconds, c_i (with $i = 1,2,3,4$) are the coefficients of primary creep, c_j (with $j = 1,2,3,4$) are the coefficients of secondary creep. This creep equation has been selected because of its ability to model both the primary and secondary creep with simple fitting coefficients. Furthermore, it is capable of predicting creep strain regardless of any coupling between time and

either stress or temperature [47]. Creep tests for BND have been performed at different temperatures but at only one stress point. Consequently, exponents c_2 and c_6 cannot be calibrated as a function of stress. Predictions are therefore meaningful only for values of Von Mises Stress close to 8.3 MPa. Linear dependency of creep has been assumed as a function of stress. In mathematical terms, coefficients $c_1 = c_6 = 1$.

A nonlinear least square optimization procedure is adopted as a first attempt to produce data fitting for the constants c_1-c_7 used in Eqn1. The primary aim is to find the value for the material constants which minimise the error to the experimental data. In mathematical terms this is expressed as the minimisation of *err* (c_1, c_2, c_3, c_4, c_5, c_6, c_7), defined in Eqn.2.

$$err = \sum_{u=1}^{m}\left(\sum_{v=1}^{n}\left(\epsilon_{cr\_exp} - \epsilon_{cr}\right)^2\right) \tag{2}$$

Where, ϵ_{cr} is the creep strain, calculated with the analytical approach of Eqn.1, ϵ_{cr_exp} is the creep strain experimentally measured, m is the number of different data sets (for different temperatures or stress values), 3 in this case, corresponding to three different temperatures, n is the number of data points of one single data set.

The nonlinear least square optimization algorithm proposed by Gong, Hyde, Sun and Hyde [33] the Levenberg-Marquadt was used and it has been implemented with the '***lsqnonlin***' command in MATLAB environment. The results of this technique are not satisfactory, as observable in Fig. 3.

Therefore, modifications to the mathematical expression of the creep law have been proposed and attempts have been conducted to find a better error minimisation, using data available in the literature for this coating system. To do that, the first observation is that the creep strain at 1473K is much higher than the one at 1373K or 1273K. For this reason, two modifications are proposed to Eqn.1:

1) If the temperature is above 1373K, Eqn1 will use $2*c_5$ instead of c_5.
2) A factor $f = \left(\frac{T}{1373}\right)^2$ has been added to Eqn.1.

The creep power law presented in Eqn.1, is thus modified as per Eqn. 3:

$$\begin{aligned} T > 1373 \quad \epsilon_{cr} &= f\frac{c_1}{c_3+1}\sigma^{c_2}t^{1+c_3}e^{\frac{-c_4}{T}} + 2fc_5\sigma^{c_6}e^{\frac{-c_7}{T}}t \\ T < 1373 \quad \epsilon_{cr} &= f\frac{c_1}{c_3+1}\sigma^{c_2}t^{1+c_3}e^{\frac{-c_4}{T}} + fc_5\sigma^{c_6}e^{\frac{-c_7}{T}}t \end{aligned} \tag{3}$$

The range of validity of Eq. (3) is one of the experimental data (1273<T<1473). When these two modifications are made, a GA optimiser [38] has been run together with Abaqus to fit the parameters. The creep model is implemented in Abaqus by using a Fortran sub-routine. The optimisation loop has been coded in MATLAB (Abaqus is called via DOS) and shown in Fig. 4.

The Abaqus FE model simulates a uniaxial creep at 8.3 MPa nominal stress for 70200 s. One side of the specimen is fully restrained (all displacements of the end face are set to zero) and the other side is loaded with a traction of 8.3 MPa. Creep strain is measured every second and the error calculated with Eq. (2). Fig. 5 gives an overview of the FE model with load and boundary conditions applied.

The results of the calibration procedure are shown in Fig. 6 and the optimum parameters are summarized in Table 1.

It can be remarked that the Abaqus predictions and the analytical formulation are giving different results, especially in the first seconds of the simulation. This is due to numerical errors. This issue is not investigated in this paper as it is out of scope.

As already remarked, the implementation of the model expressed in Eqn.3 is done in Abaqus by using a Fortran sub-routine. Although this allows flexibility and precision of structural analysis, it is not beneficial in terms of computational running time. If the required precision for design purpose is reached without the use of a Fortran sub-routine this would be beneficial. For this reason, the creep experimental data of the EBC have been modelled with a simple power low of the form expressed in Eqn.4.

$$\frac{d\epsilon_{cr}}{dt} = A\sigma^a t^b \tag{4}$$

Where a, b are exponents and A is a multiplier, in other words fitting parameters.

The same optimisation tool (Abaqus MATLAB loop) has been used to optimise the fitting parameters. Their value is given in Table 2. Also in this case, as already done for the BDN, the von mises exponent has been left equal to 1, as the dependency on stress cannot be extracted from experimental results.

The results of the fitting are given in Fig. 7.

Experimental data of the EBC have been obtained for a range of temperatures different then the BND. The fitting is considered satisfactory for design purposes. In Fig. 7, error minimization between the experimental data and the model are shown at different temperatures. The proposed calibration is still not fully capable of exactly following the shape of the experimental data curves for lower temperatures (1073 K, 1123 K). The creep strain is in fact first underpredicted and then over

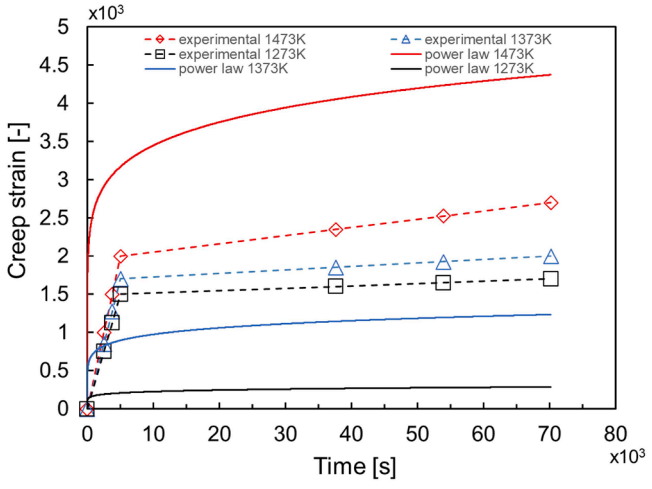

Fig. 3. Results of the first data fitting attempt with the "traditional" power low of Eq. (1).

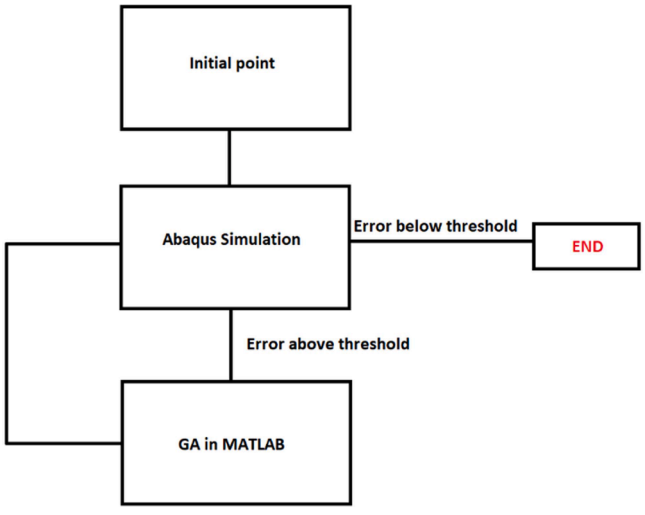

Fig. 4. Optimisation Tool for calibrating the parameters of the modified creep power law for the bond coat.

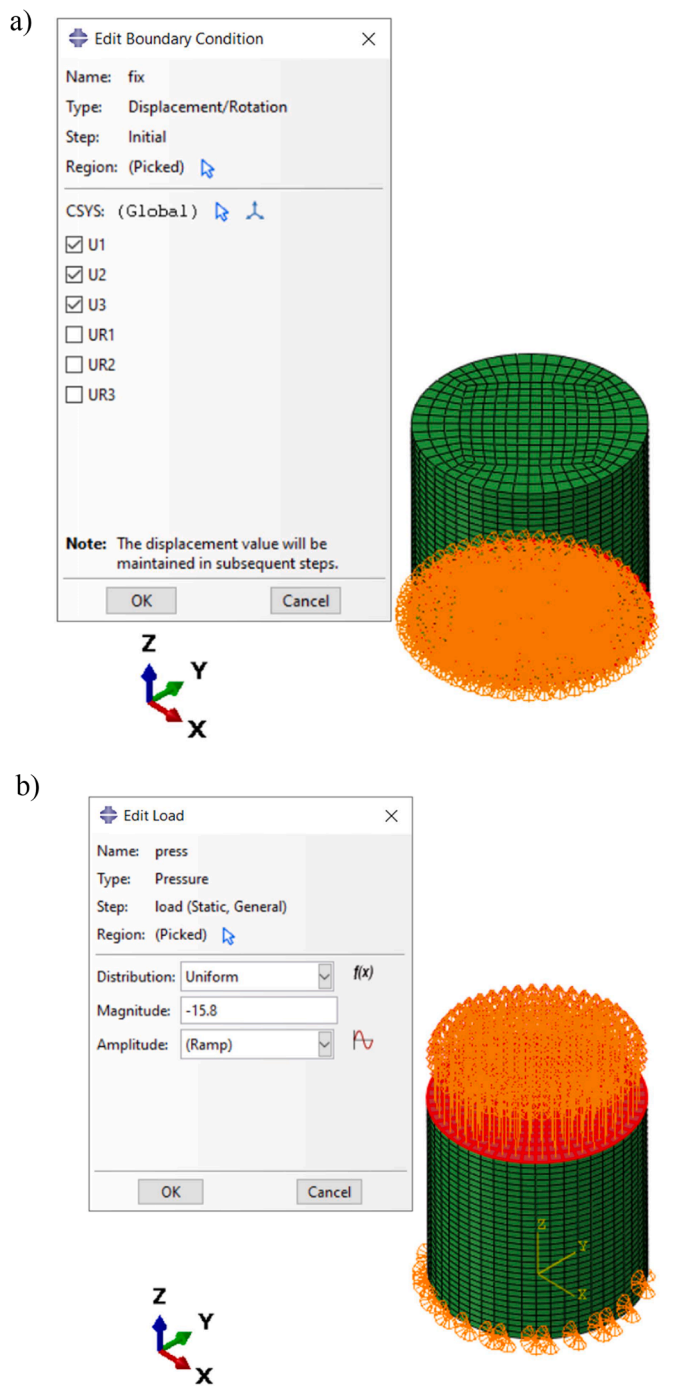

Fig. 5. (a) Boundary Condition at the bottom surface; (b) Traction at the top surface.

predicted after 50000 s exposure time. However, the model can give conservative results for longer creep exposure (time greater than 50000 seconds) and the error for long time exposure is in any case within 10%, result acceptable for engineering design and assessment. More importantly, when modelling the high temperature behavior (1173 K), the error for long exposure time is below 1% and the shape of the experimental curve is well caught by the model. The power law, furthermore, does not need a Fortran sub-routine to be implemented in Abaqus and it is much faster in producing analysis results.

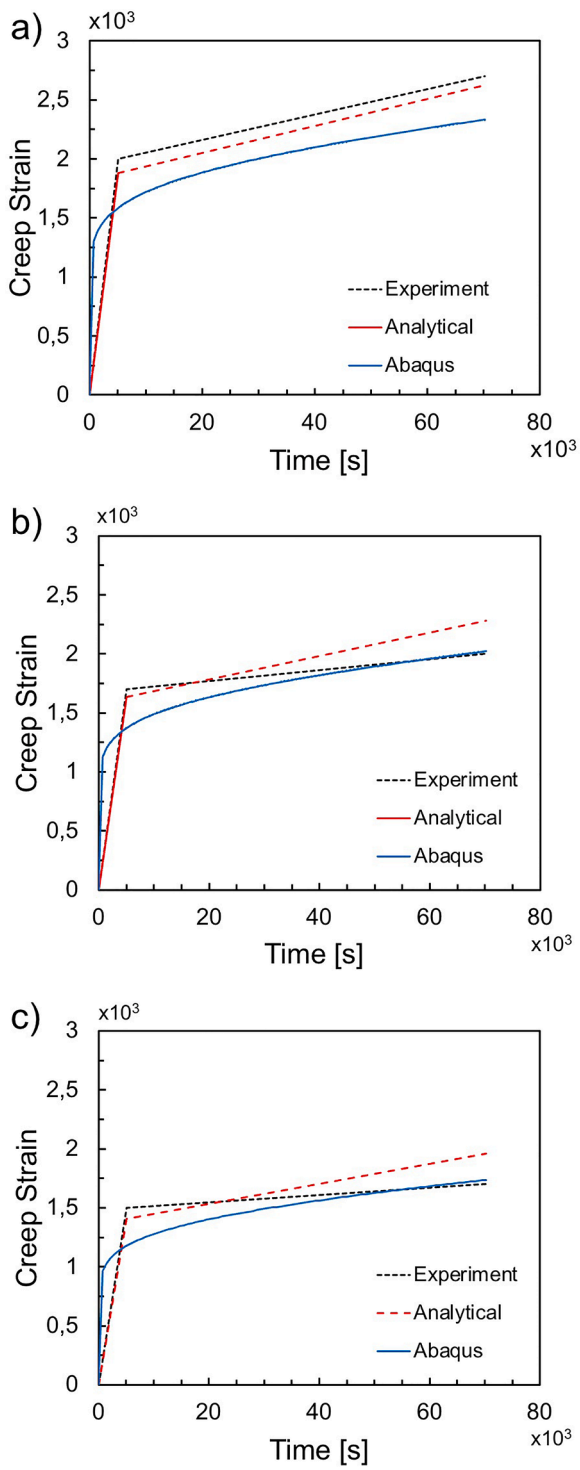

Fig. 6. Data fitting with the new proposed formulation: (a) 1473 K; (b) 1373 K; (c) 1273 K.

3. Optimization of the layers thickness

The High-Pressure Turbine components are subjected to severe temperature gradients during transient conditions. Coating failures, including loss and spallation, has been in fact observed in service [39]. It is therefore important to reduce in plane interface stresses between each layer of the three constituents of the coating: LAY3, EBC and BND [39]. Transient stresses are a function of the elastic and thermal properties of

Table 1
Optimum parameters for BND creep (primary and secondary).

c_1	1020
c_2	1
c_3	-0.91
c_4	25600
c_5	200
c_6	1
c_7	37000

Table 2
Optimum parameters for LAY3 creep (primary and secondary).

A	*a*	*b*	*T*
1.01716e-06,	1	-0.68	1073
1.52516e-06,	1	-0.68	1123
4.3959e-05,	1	-0.98	1173
5.8514e-05,	1	-0.98	1473

each coating layer. A coating structure with different layers will have a different thermal response and therefore a different stress distribution at the interface. The value of the thickness of each layer influences the magnitude of these stresses, therefore it is crucial for the integrity of the component the evaluation of the optimal configurations of the three-layered coating, which minimise the peak in-plane stress at the interface. The DoE procedure was used to determine the thickness of each layer in a coated CMC component. Three possible thicknesses were defined for each layer. The selected values are summarized in Table 3.

The thickness of the CMC substrate is a constant and not considered as variable. To investigate which thickness combination gives the lowest interface stresses, a worst Principal Stress (WPS) of the virtual experiment has been built. The stress considered in WPS is the one causing the crack initiation on the coating system. It has been taken in the mid-node of the cross section (to avoid edge effects, which are already small in this case). In the design of experiment procedure, considering the three coating layers which can assume 3 discrete values of the thickness each, a full factorial plan consisting of total of $3^3 = 27$ specimens ($l^n = 3^3$, where l is the number of levels for the variables and n is the number of variables) was designed. The specimens will differ each other only for their coating thickness layers, th_{LAY3}, th_{EBC}, th_{BND}, for the LAY3, EBC and BND layers, respectively (Table 4). The complete list of specimens (and corresponding FE Models) is given in Table 4.

The virtual specimen is shown in Fig. 8.

Virtual specimen dimensions are given in Table 5. The frame of reference used is the one shown in Fig. 8.

The optimal configuration of the layers' thicknesses, able to minimise the interface stress between the layers (LAY3/EBC, EBC/BND and BND/CMC interface) is searched by simulating the twenty-seven scenarios. FE Modelling is described in Section 3.1. Results are given in Section 3.2

3.1. FE modelling

The thermal transient (heating up) has been modelled as an explicit Abaqus thermal analysis. Thermal maps (temperatures at each node) have been exported every 0.1 s. The thermal maps have been then applied to a stress analysis (a series of quasi-static analyses, each every 0.1s). The same mesh has been used for thermal and stress analyses. HEX20 elements have been used, with a 0.1 mm size. A minimum of 3 through-the-thickness elements have been applied to every layer of the coating. The thermal top surface boundary condition is shown in Fig. 9. A temperature (1300°C) is imposed.

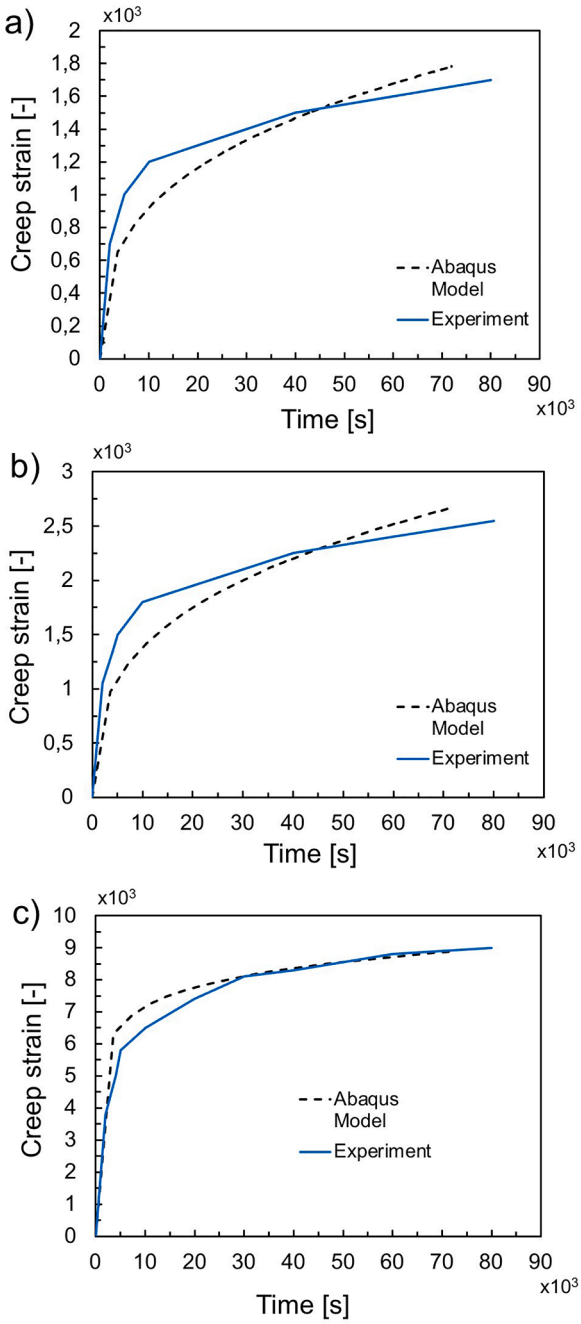

Fig. 7. EBC creep data fitting results: (a) 1073 K; (b) 1123 K; (c) 1173 K.

Table 3
Coating thickness layer design options.

	level 1 [mm]	level 2 [mm]	level 3 [mm]
LAY3	0.4	0.5	0.6
EBC	0.15	0.25	0.35
BND	0.05	0.1	0.15

A film condition to represent air forced convection (film coefficient 0.01 mW/mm^2/K) [44] and a radiation condition (emissivity 0.85) [40] to model the energy dissipated by irradiation have been used for the bottom surface (Fig. 10).

The thermal problem is treated as a 1D problem (no temperature distortion at the edges). Twenty-seven (27) different thermal transients have therefore been obtained. The output of these models are nodal

Table 4
Complete list of virtual specimens and corresponding FE models.

Configurations	th_{LAY3}	th_{EBC}	th_{BND}
1	0.5	0.25	0.1
2	0.6	0.25	0.1
3	0.4	0.25	0.1
4	0.5	0.15	0.1
5	0.6	0.15	0.1
6	0.4	0.15	0.1
7	0.5	0.35	0.1
8	0.6	0.35	0.1
9	0.4	0.35	0.1
10	0.5	0.25	0.15
11	0.6	0.25	0.15
12	0.4	0.25	0.15
13	0.5	0.15	0.15
14	0.6	0.15	0.15
15	0.4	0.15	0.15
16	0.5	0.35	0.15
17	0.6	0.35	0.15
18	0.4	0.35	0.15
19	0.5	0.25	0.05
20	0.6	0.25	0.05
21	0.4	0.25	0.05
22	0.5	0.15	0.05
23	0.6	0.15	0.05
24	0.4	0.15	0.05
25	0.5	0.35	0.05
26	0.6	0.35	0.05
27	0.4	0.35	0.05

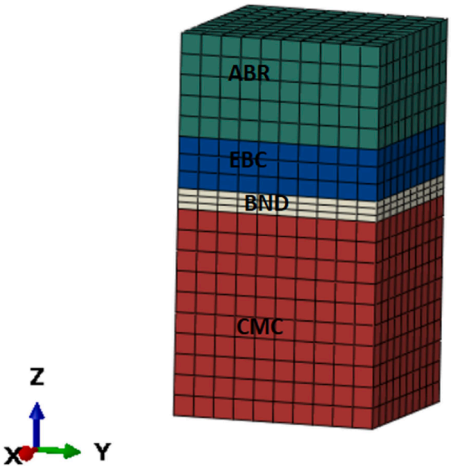

Fig. 8. Virtual specimen for the Design of Experiment trials to minimize the interface stresses.

Table 5
Virtual specimen dimensions.

	x – dimension	y – dimension	z – dimension
LAY3	1	1	th_{LAY3}
EBC	1	1	th_{EBC}
BND	1	1	th_{BND}
CMC	1	1	1

temperatures. Nodal temperatures have been exported to a thermal model (map exported every 0.1 s). Steady state stress analyses have been performed from 0.1 s to 2s of the transient, with an interval of 0.1 s. The only boundary condition applied is a fix point on the bottom surface mid-point. The output of the stress models is a set of stress values at the interface (stress is taken in the mid-section node to discard the edge effects. Stress values are available every 0.1 s from 0 to 2 s. Thermo-mechanical properties have been taken from the open literature [30,

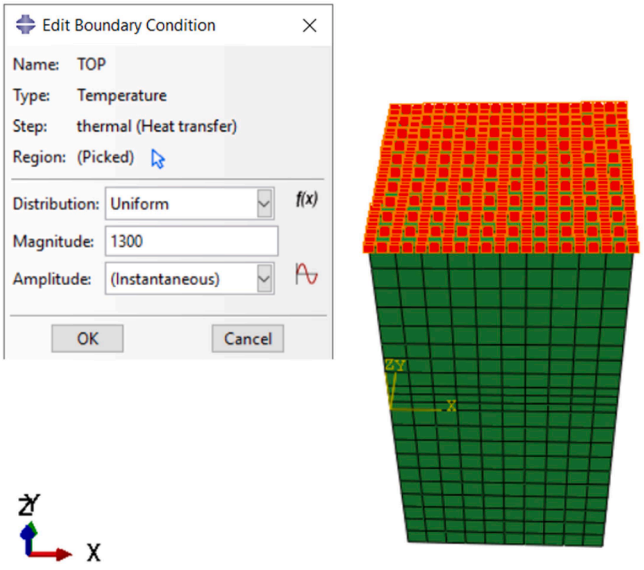

Fig. 9. Thermal model top surface boundary condition; 1300°C.

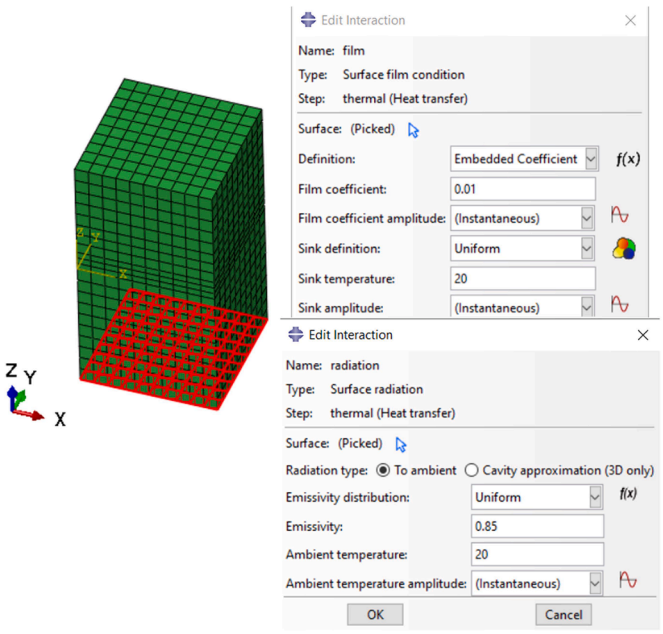

Fig. 10. Thermal model bottom surface film and radiation condition.

Table 6
LAY3 thermo-mechanical properties as a function of temperature.

	20°C	**1300**°C
Stiffness Modulus E [MPa]	33400	26720
Poisson's ratio ν	0.3	0.3
Thermal conductivity c [mW/mm/K]	1.60	1.20
Density ρ [Mg/mm^3]	$5.32*10^{-9}$	$5.32*10^{-9}$
Thermal expansion coefficient α [1/K]	$4.95*10^{-6}$	$6.05*10^{-6}$
Specific heat [mJ/Mg/K]	$4.40*10^{8}$	$4.64*10^{8}$

31,41–45]. No contact conditions were defined between the layers but equivalence of nodes in the Finite Elements Model. The different coating layers are in fact bonded together with no possibility of free relative movement [48,49]. LAY3 data is available in Table 6. EBC is Table 7. BND in Table 8 and CMC substrate in Table 9. Data is linearly

Table 7
EBC thermo-mechanical properties as a function of temperature.

	20°C	**1300**°C
Stiffness Modulus E [MPa]	150000	120000
Poisson's ratio ν	0.2	0.2
Thermal conductivity c [mW/mm/K]	2.00	1.50
Density ρ [Mg/mm^3]	$6.65*10^{-9}$	$6.65*10^{-9}$
Thermal expansion coefficient α [1/K]	$3.50*10^{-6}$	$5.50*10^{-6}$
Specific heat [mJ/Mg/K]	$5.50*10^{8}$	$6.05*10^{8}$

Table 8
BND thermo-mechanical properties as a function of temperature.

	20°C	**1300**°C
Stiffness Modulus E [MPa]	97000	89046
Poisson's ratio ν	0.21	0.21
Thermal conductivity c [mW/mm/K]	20.00	15.00
Density ρ [Mg/mm^3]	$2.33*10^{-9}$	$2.33*10^{-9}$
Thermal expansion coefficient α [1/K]	$3.50*10^{-6}$	$5.00*10^{-6}$
Specific heat [mJ/Mg/K]	$7.00*10^{8}$	$7.70*10^{8}$

Table 9
BND thermo-mechanical properties as a function of temperature.

	20°C	**1300**°C
Stiffness Modulus E_x [MPa]	345000	320850
Stiffness Modulus E_y [MPa]	345000	320850
Stiffness Modulus E_z [MPa]	251850	193601
Stiffness Modulus G_{xy} [MPa]	151800	99029
Stiffness Modulus G_{xz} [MPa]	151800	99029
Stiffness Modulus Gy_z [MPa]	110000	84174
Poisson's ratio ν_{xy}	0.15	0.15
Poisson's ratio ν_{xz}	0.15	0.15
Poisson's ratio vyz	0.15	0.15
Thermal conductivity c_x [mW/mm/K]	45.00	34.00
Thermal conductivity c_y [mW/mm/K]	45.00	34.00
Thermal conductivity c_z [mW/mm/K]	33.00	25.00
Density ρ [Mg/mm^3]	$3.00*10^{-9}$	$2.33*10^{-9}$
Thermal expansion coefficient α_x [1/K]	$3.90*10^{-6}$	$4.60*10^{-6}$
Thermal expansion coefficient α_y [1/K]	$3.90*10^{-6}$	$4.60*10^{-6}$
Thermal expansion coefficient α_z [1/K]	$4.10*10^{-6}$	$4.80*10^{-6}$
Specific heat [mJ/Mg/K]	$6.70*10^{8}$	$7.20*10^{8}$

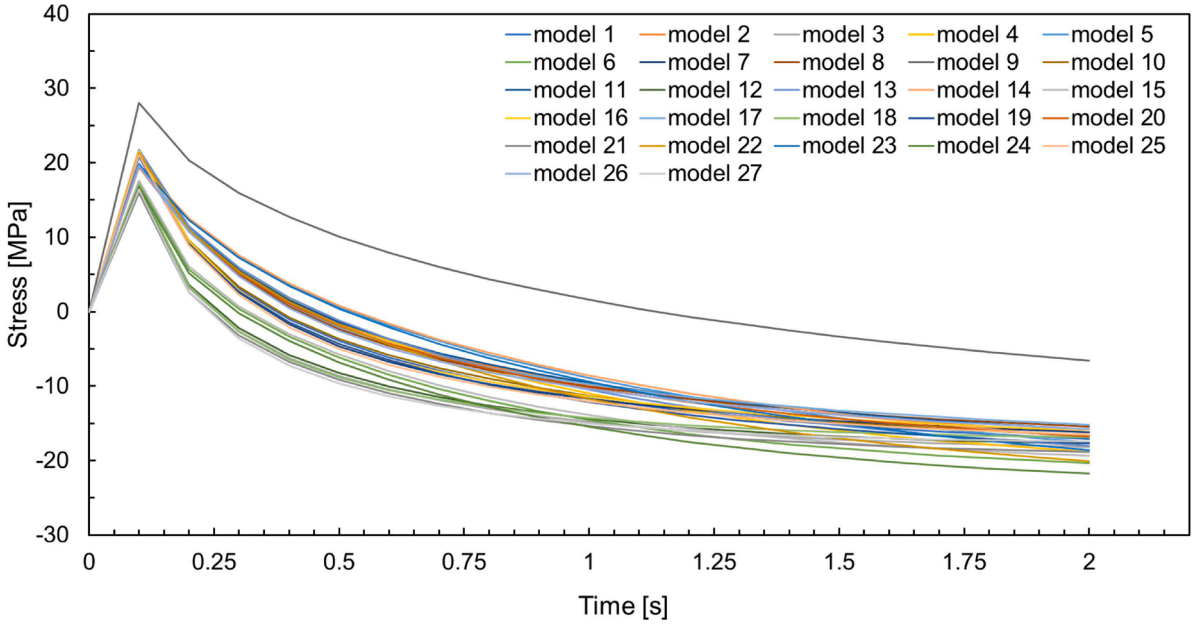

Fig. 11. LAY3/EBC Worst Principal Stress during thermal transient (heating up).

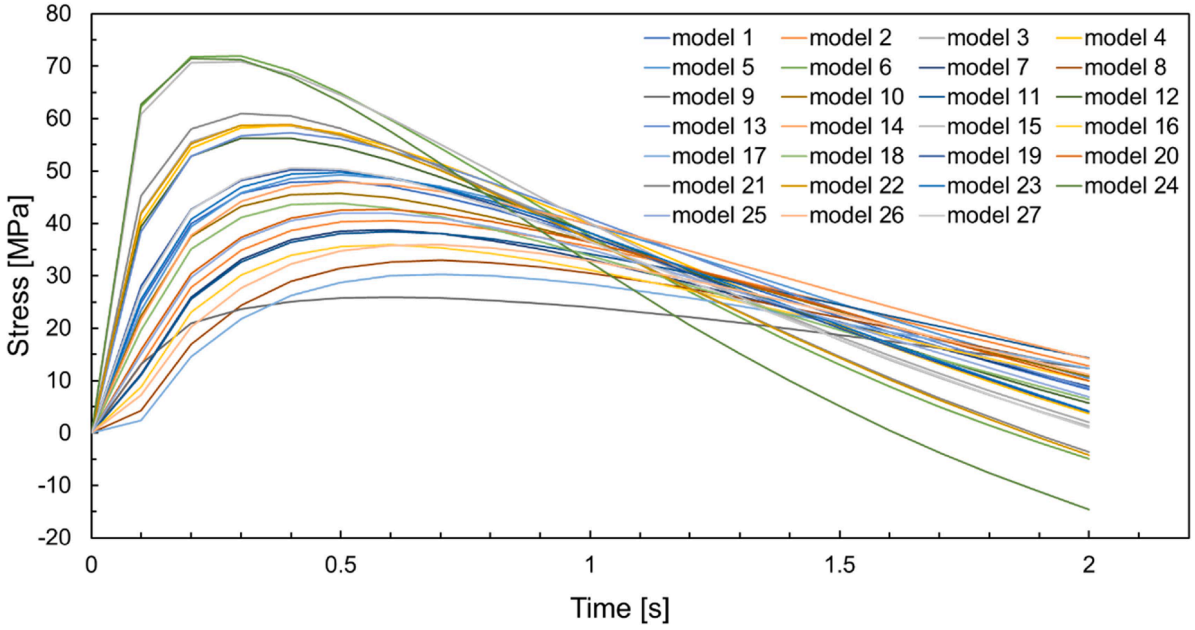

Fig. 12. EBC/BND Worst Principal Stress during thermal transient (heating up).

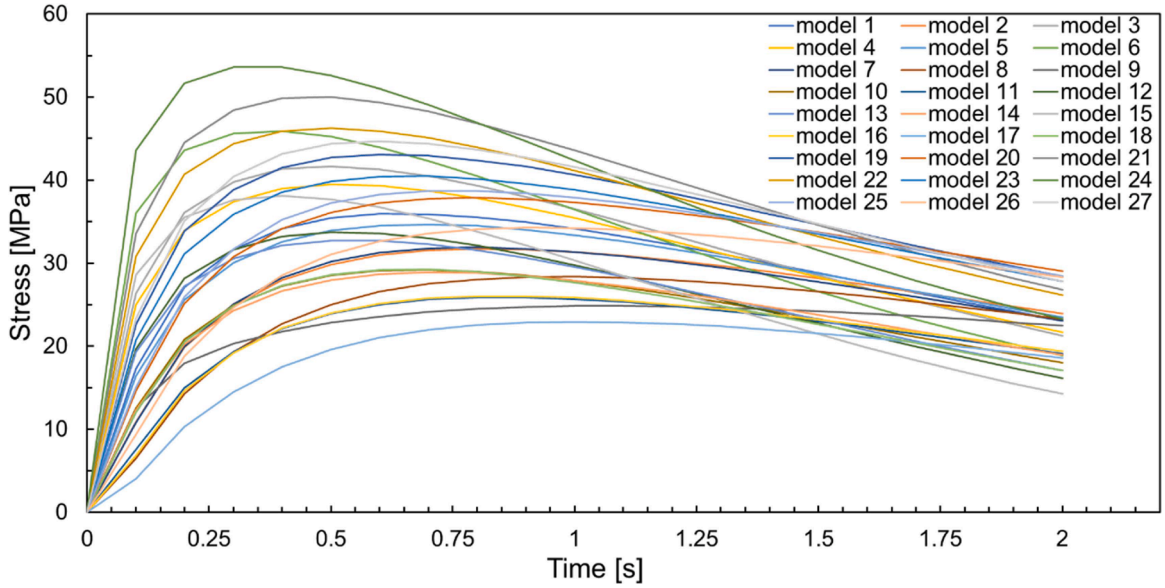

Fig. 13. BND/CMC Worst Principal Stress during thermal transient (heating up).

interpolated between 20 and 1300°C.

CMC properties are defined via directional engineering constants along the axes *x, y* and *z* shown in Fig. 8.

3.2. Results

The stress response at the interface is the main result of interest of the models. Stress time dependency (stress history) is important when evaluating the coating. During thermal transient, the stress at the LAY3/EBC and EBC/BND interface increases with time until a maximum value is reached. When the temperature gets more uniform, the interface stress tends to decrease and stabilise. For the BND/CMC interface, the interface stress tends to increase until a maximum value is reached at the end of transient. The worst in plane principal stress at the layer interfaces, is shown in this section. The interface stresses between LAY3 and EBC, between EBC and BND, and between BND and CMC are given in Fig. 11, Fig. 12 and Fig. 13, respectively, while the stresses on the CMC substrate are shown in Fig. 14.

To rank the 27 models, in other words to establish a performance, a fitness function of the design solution, the minimum non-negative stress is extracted from the plots (excluding time 0, where no stress state exists). The extracted minimum non-negative stress values at the three interfaces (namely LAY3/EBC, EBC/BND, and BND/CMC) are reported in Table 10.

Configuration 27 is the one giving the best results for LAY3/EBC interface. The best result is obtained by decreasing the thickness of LAY3 and increasing the thickness of EBC. Results are more sensible to the thickness of the LAY3 than to the EBC and BND thickness. To prove this concept, let the interface stress of model 25, 26 and 27 be compared (Fig. 15).

A 25% difference can be appreciated in the peak stress between 0.5 mm LAY3 thickness (model 25) and 0.6 mm LAY3 thickness (model 27).

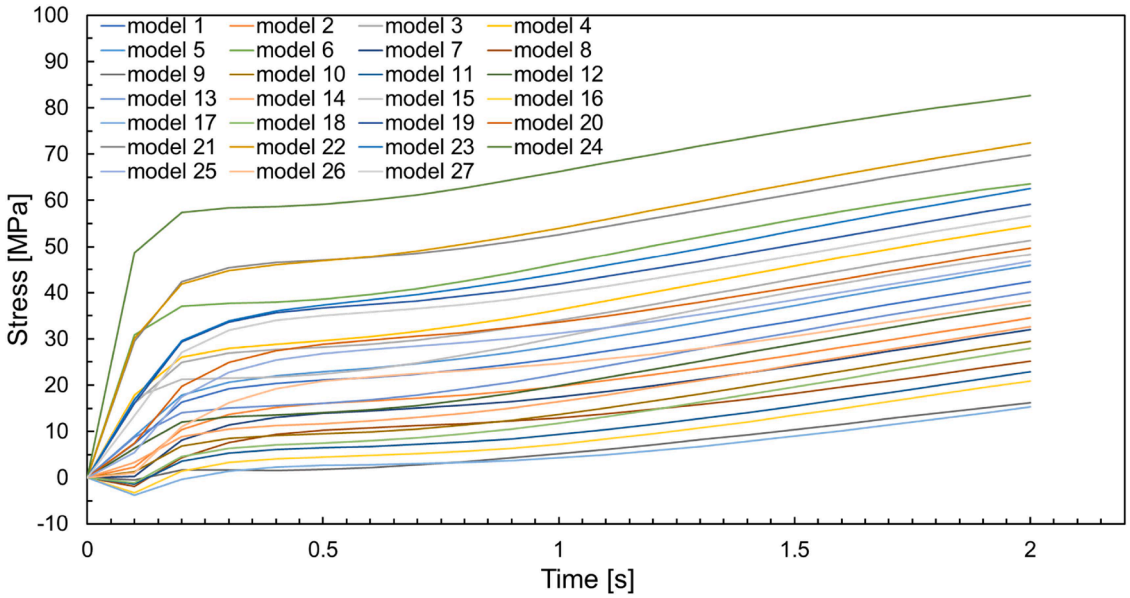

Fig. 14. CMC Substrate Worst Principal Stress during thermal transient (heating up).

Table 10
Minimum non-negative worst principal stress at the three interfaces, LAY3/EBC, EBC/BND, BND/CMC for the 27 configurations tested.

Configurations	LAY3/EBC	EBC/BND	BND/CMC
1	21.1	48.04	35.92
2	19.58	40.59	31.72
3	16.42	58.77	41.66
4	21.57	58.66	39.5
5	19.79	49.23	34.68
6	17.26	71.93	45.9
7	21.36	38.73	31.89
8	19.76	32.93	28.35
9	28.03	25.95	24.85
10	21.33	45.75	29.2
11	19.72	38.42	25.87
12	16.8	56.24	33.73
13	21.73	57.32	32.73
14	19.86	47.82	28.88
15	17.6	70.85	38.09
16	21.56	35.88	26.03
17	19.89	30.31	22.92
18	17.13	43.87	29.25
19	20.83	50.2	43.08
20	19.42	42.63	37.86
21	15.96	60.96	49.97
22	21.37	58.82	46.24
23	19.74	49.78	40.47
24	16.78	71.5	53.59
25	21.11	41.95	38.71
26	19.6	35.93	34.29
27	16.41	50.51	44.68

If, on the other hand, we consider the models with $th_{LAY3} = 0.4$ and $th_{BND} = 0.05$ (model 21, 24 and 27), we can observe that the difference in peak stress is much lower (Fig. 16).

When looking at the EBC/BND interface, the model with lower stress is Model 9 (see Table 5 for the details of layers thickness). Also in this case, as per model 27, $th_{LAY3} = 0.4$ and $th_{EBC} = 0.35$. Second ranked is model 8, and third ranked is model 7. These three models differ only for the LAY3 thickness and have all $th_{BND} = 0.1$. If $th_{BND} = 0.05$ (Model 27), a massive stress increase is instead observed. This implies, as expected, that BND thickness plays an important role for this interface. Comparative results of these models (7, 8, 9 and 27) are given in Fig. 17.

When looking at the BND/CMC interface, the model with lower stress is Model 17. In this case, $th_{LAY3} = 0.6$ and $th_{EBC} = 0.35$. However,

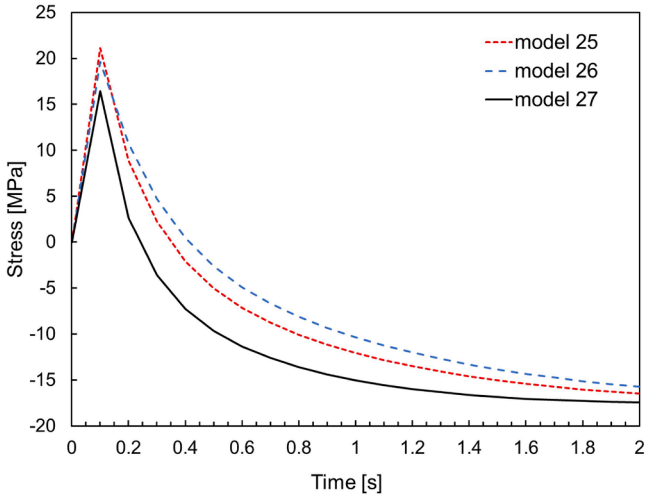

Fig. 15. LAY3/EBC Interface Worst Principal Stress during thermal transient (heating up) – Model 25, 26 and 27 in isolation.

model 9 is second ranked in stress performance for this interface. Model 9 is also the best one for the CMC substrate itself (Fig. 14). It is therefore concluded that the best design solution of the Design of Experiments is $th_{LAY3} = 0.4$, $th_{EBC} = 0.35$ and $th_{BND} = 0.1$. This comes from taking the minimum of the sum of fitness values in Table 10.

It has been found that the thickness of LAY3 layer has a strong effect on the thermal and mechanical response. With the adopted material properties, it has been found that reducing the LAY3 thickness may be beneficial. BND thickness lays a role in the EBC/BND interface integrity. It must however be remarked that the results are strongly dependent on the material properties itself. These conclusions are quite sensitive to the material properties used. For this reason, the results need to be taken by the reader as qualitative and not conclusive to describe the actual behaviour of the coated CMC component. Being aware of the sensitivity of the results with respect to material properties, a combinatorial design of experiments procedure has been preferred to a proper optimisation [46], either gradient based or with heuristic techniques. In case the material properties are well established, an optimization with TGO and silica depletion constraints could be proposed instead and will be a part

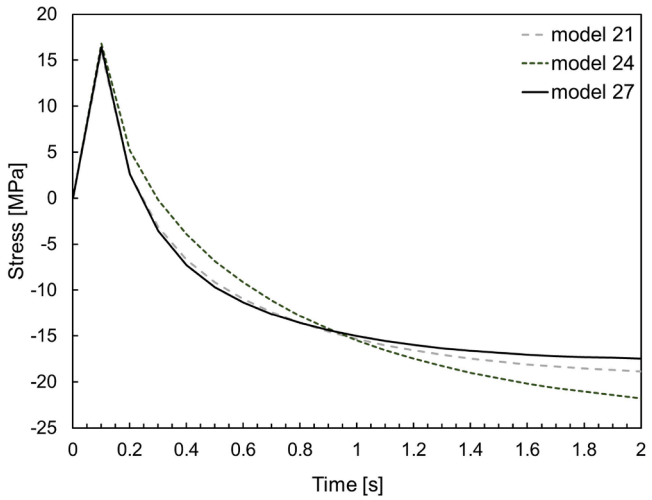

Fig. 16. LAY3/EBC Interface Worst Principal Stress during thermal transient (heating up) – Model 21, 24 and 27 in isolation.

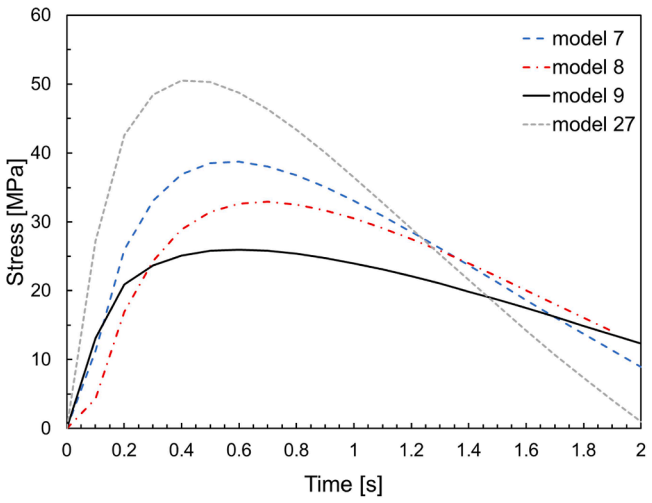

Fig. 17. EBC/BND Interface Worst Principal Stress during thermal transient (heating up) – Model 7, 8, 9 and 27 in isolation.

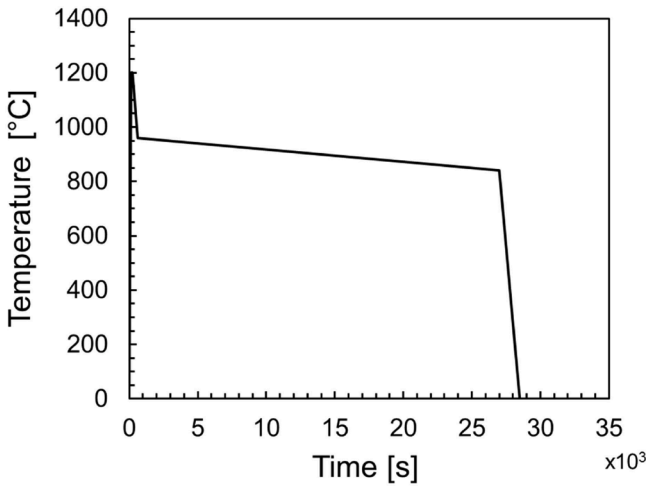

Fig. 18. Temperature scale factor during a flight profile.

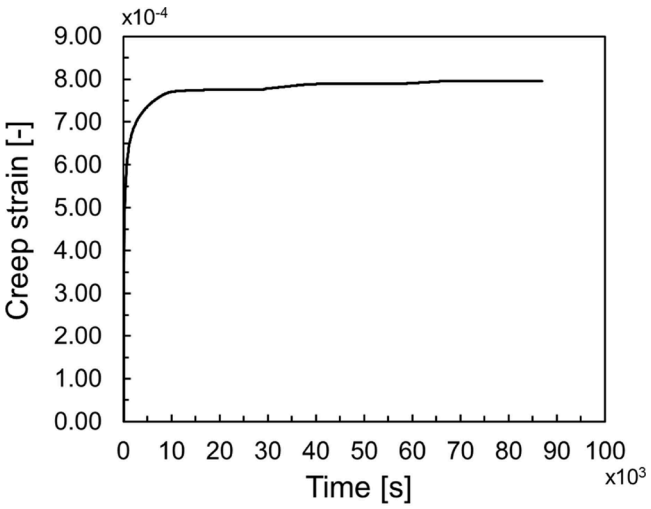

Fig. 19. Creep Strain during 3 flights at the LAY3/EBC interface.

of future work. The value of the design of experiment here proposed can be, however, the basis of any design options.

4. Using the inelastic calibration to establish the structural performance of the optimum coating

The two aspects treated in this work are combined to give an analysis procedure of the coating stress with inelastic material properties. Three consecutive flight profiles [29] are simulated with inelastic material properties (creep properties calculated in Section 2) to show inelastic strains. It is important to remark, then any contribution to the deformation is crucial for the design of these applications. Gaps and tip clearances are a strong influence on the engine performance and stability. The design solution chosen is the "configuration 9" individuated by the DoE. Model 9 is therefore subjected to a uniform temperature profile (1200°C) as shown in Fig. 18.

This flight profile has the duration of 29000 s, and it is repeated 3 times during the simulation. The inelastic creep strain at the interface is given in Fig. 19.

Creep deformation is mainly driven, as expected, by the initial primary creep. Strain keeps increasing but with a very small rate. It is remarked that the initial Residual Stresses due to the spray operation (manufacturing) have not been considered in this qualitative simulation. Creep strain is mainly caused by the primary creep during the first flight cycle. Secondary creep slope is quite small as expected for the low level of stress. Two points are however worth of a remark. The first one is that multiple flight profiles (the entire flight duration) shall be modelled when trying to predict creep behavior of coatings. This, although computationally expensive, is facilitated by the diffusion of HPC (High Performance Computing). The second point is that the creep inelastic strain results are strongly dependent on the stress assumption (linear in the formulation adopted in this work). This hypothesis shall be investigated as a part of future work.

5. Conclusions

Ceramic matrix composite (CMC) components could be truly a game changer in the power generation industry, Aerospace and Defence. Coating technology is fundamental in protecting the components from environment and from thermal shocks.

Creep simulations are extremely important in the design phase to understand non-linear deformation and stress relaxation of coatings. This also implies a better understanding of the residual stress field induced by the manufacturing process. Open literature creep data of CMC coating layers, Environment Barrier Coating (EBC) and silicon

bond (BND), have been implemented into an Abaqus card and here reported. A modified power law for primary and secondary creep has been used. A rigorous optimization procedure has been used to interpolate the mathematical fitting and calculate the coefficients of the creep law, and material card data made available. It must be highlighted that the silicon bond creep strain is lower that the EBC one. The anomaly, however, can be ascribed to the original experimental data rather than to the creep law optimization developed in the present work.

The high thermal gradients during the heating up and cooling down phases may induce cracks at the coating interfaces or between CMC and coating layers. For this reason, it is important to design the thickness of each layer constituent in such a way to minimize the interface stresses. A design of experiment procedure was adopted to analyse the temperature heating up transitory. The design space of different values of thickness layers of the softer layer 3 (LAY3), the EBC and BND has been explored to find the best coating design solution, the one minimising the interface stress during extreme aero-engine high pressure turbine thermal transient conditions. It has been found that reducing the thickness of the LAY3 layer and increasing the thickness of the EBC is beneficial to reduce the in-plane interface stresses. However, the results found are only true for the set of material properties used and the results (and therefore the design solution) is strongly influenced by the material data available. Furthermore, the cooling down process will be considered for future works. It is also important to remark that together with the thickness, manufacturing constraint on the thickness of each layer should be considered in the case of complex geometries. Lastly, the edge effect that could arise in a real component shall be investigated analysing the thermal transient (heating up and cooling down) or a real component (a High-Pressure Turbine Seal Segment for example).

CRediT authorship contribution statement

Giacomo Canale: Writing – original draft, Methodology, Investigation, Formal analysis, Conceptualization. **Felice Rubino:** Writing – review & editing, Writing – original draft, Formal analysis, Data curation, Conceptualization. **Roberto Citarella:** Supervision, Methodology, Conceptualization.

Declaration of competing interest

The authors declare that they have no known competing financial interests or personal relationships that could have appeared to influence the work reported in this paper.

Data availability

Data will be made available on request.

Acknowledgments

The authors would like to thank Dr Steven Pattison of Rolls-Royce plc and Lynn Powers of Rolls-Royce Corporations for their ongoing support.

References

[1] R.P. Panakarajupally, F. Mirza, J. El Rassi, G.N. Morscher, F. Abdi, S. Choi, Solid particle erosion behavior of melt-infiltrated SiC/SiC ceramic matrix composites (CMCs) in a simulated turbine engine environment, Compos. Part B Eng. 216 (2021) 108860, https://doi.org/10.1016/j.compositesb.2021.108860.
[2] P. Barnard, M.B. Henderson, N. Rhodes, CMC integration and demonstration for gas turbine engines (CINDERS), Appl. Therm. Eng. 24 (2004) 1755–1764, https://doi.org/10.1016/j.applthermaleng.2003.11.019, 11–12.
[3] Z. Yang, W. Li, Y. Chen, W. Zeng, W. Chen, X. Cao, Life assessment of thermomechanical fatigue in a woven SiC/SiC ceramic matrix composite with an environmental barrier coating at elevated temperature, Int. J. Fatigue 172 (2023) 107584, https://doi.org/10.1016/j.ijfatigue.2023.107584.
[4] J.T. Winowlin Jappes, A. Ajithram, M. Adamkhan, D. Reena, Welding on Ni based super alloys–a review, Mater. Today Proc. 60 (2022) 1656–1659, https://doi.org/10.1016/j.matpr.2021.12.208.
[5] R. Wang, K. Jiang, F. Jing, D. Hu, Thermomechanical fatigue failure investigation on a single crystal nickel superalloy turbine blade, Eng. Fail. Anal. 66 (2016) 284–295, https://doi.org/10.1016/j.engfailanal.2016.04.016.
[6] O.G. Diaz, D.A. Axinte, P. Butler-Smith, D. Novovic, On understanding the microstructure of SiC/SiC Ceramic Matrix Composites (CMCs) after a material removal process, Mater. Sci. Eng. A Struct. 743 (2019) 1–11, https://doi.org/10.1016/j.msea.2018.11.037.
[7] A.F. El-Sayed, Aircraft Propulsion and Gas Turbines Engines, 2nd ed., CRC Press, Boca Raton, 2017.
[8] H.E. Eaton, G.D. Linsey, Accelerated oxidation of SiC CMC's by water vapor and protection via environmental barrier coating approach, J. Eur. Ceram. Soc. 22 (2002) 2741–2747, https://doi.org/10.1016/S0955-2219(02)00141-3.
[9] X. Cao, X. Luan, Y. Wang, Z. Zhang, Ji. Li, G. Han, L. Cheng, Oxidation and corrosion behavior of 2D laminated SiC/SiC with Si/mullite/BSAS EBC in dry oxygen/water vapor at 1200°C, Corros. Sci. 219 (2023) 111237, https://doi.org/10.1016/j.corsci.2023.111237.
[10] J. Huang, R. Liu, Q. Hu, X. Guo, G. Li, Y. Tu, X. Lu, M. Xu, L. Deng, J. Jiang, S. Dong, L. Liu, M. Chen, X. Cao, High temperature abradable sealing coating for SiCf/SiC ceramic matrix composites, Ceram. Int. 49 (2023) 1779–1790, https://doi.org/10.1016/j.ceramint.2022.09.141.
[11] F. Rubino, D. Merino, A.T. Silvestri, C. Munez, P. Poza, Mechanical properties optimization of Cr3C2-NiCr coatings produced by compact plasma spray process, Surf. Coat. Technol. 465 (2023) 129570, https://doi.org/10.1016/j.surfcoat.2023.129570.
[12] F. Rubino, D. Merino-Millan, F. Tucci, P. Poza, Mechanical optimisation of Ni coatings produced by low-pressure cold spray, Surf. Eng. 39 (2023) 653–665, https://doi.org/10.1080/02670844.2023.2257357.
[13] F. Rubino, D. Merino, C. Munez, P. Poza, Evaluating the corrosion resistance of inconel 625 coatings, processed by compact plasma spray, for applications in concentrating solar power plants, Key Eng. Mater. 926 (2022) 1736–1745, https://doi.org/10.4028/p-d3uuc2.
[14] F. Rubino, P. Poza, G. Pasquino, P. Carlone, Thermal spray processes in concentrating solar power technology, Metals 11 (9) (2021) 1377, https://doi.org/10.3390/met11091377. Basel.
[15] A. Viscusi, A. Astarita, R.D. Gatta, F Rubino, A perspective review on the bonding mechanisms in cold gas dynamic spray, Surf. Eng. 35 (2019) 743–771, https://doi.org/10.1080/02670844.2018.1551768.
[16] F. Rubino, A. Astarita, P. Carlone, Thermo-mechanical finite element modeling of the laser treatment of titanium cold-sprayed coatings, Coatings 8 (6) (2018) 219, https://doi.org/10.3390/coatings8060219.
[17] V. Paradiso, F. Rubino, F. Tucci, A. Astarita, P. Carlone, "Thermo-mechanical modeling of laser treatment on titanium cold-spray coatings, AIP Conf. Proc. (2018) 100011, https://doi.org/10.1063/1.5034951, 1960.
[18] F. Rubino, V. Paradiso, A. Astarita, P. Carlone, A. Squillace, Advances in titanium on aluminium alloys cold spray coatings, in: P. Cavaliere (Ed.). Cold-Spray Coatings: Recent Trends and Future perspectives, Springer, Cham, 2017, pp. 225–249, https://doi.org/10.1007/978-3-319-67183-3_7.
[19] P. Carlone, A. Astarita, F. Rubino, N. Pasquino, P. Aprea, Selective laser treatment on cold-sprayed titanium coatings: numerical modeling and experimental analysis, Metall. Mater. Trans. B 47 (2016) 3310–3317, https://doi.org/10.1007/s11663-016-0636-7.
[20] F. Rubino, A. Astarita, P. Carlone, S. Genna, C. Leone, F.M. Capece Minutolo, A. Squillace, Selective laser post-treatment on titanium cold spray coatings, Mater. Manuf. Process. 31 (2016) 1500–1506, https://doi.org/10.1080/10426914.2015.1037912.
[21] A. Astarita, F. Rubino, P. Carlone, A. Ruggiero, C. Leone, S. Genna, M. Merola, A. Squillace, On the improvement of AA2024 wear properties through the deposition of a cold-sprayed titanium coating, Metals 6 (8) (2016) 185, https://doi.org/10.3390/met6080185. Basel.
[22] F. Rubino, P. Ammendola, A. Astarita, F. Raganati, A. Squillace, A. Viscusi, R. Chirone, L. Carrino, An innovative method to produce metal foam using cold gas dynamic spray process assisted by fluidized bed mixing of precursors, Key Eng. Mater. (2015) 913–918, https://doi.org/10.4028/www.scientific.net/KEM.651-653.913, 651-653.
[23] A Astarita, S. Genna, C. Leone, F.M. Capece Minutolo, F. Rubino, A. Squillace, Study of the laser remelting of a cold sprayed titanium layer, Proc. CIRP 33 (2015) 452–457, https://doi.org/10.1016/j.procir.2015.06.101.
[24] H. Wang, Criteria for analysis of abradable coatings, Surf. Coat. Technol. 79 (1996) 71–75, https://doi.org/10.1016/0257-8972(95)02443-3.
[25] C. Bringhenti, J.R. Barbosa, Effects of turbine tip clearance on gas turbine performance, in: Proceedings of the ASME Turbo Expo: Power for Land, Sea, and Air 6, 2008, pp. 1715–1721, https://doi.org/10.1115/GT2008-50196.
[26] D. Tejero-Martin, A. Rincon Romero, R.G. Wellman, T. Hussain, "Interaction of CMAS on thermal sprayed ytterbium disilicate environmental barrier coatings: a story of porosity", Ceram. Int. 48 (2022) 8286–8296.
[27] P.C. Ruffles, The History of the Rolls-Royce RB211 Turbofan Engine, The Rolls-Royce Heritage Trust, Derby, 2014.
[28] J.G. Odhiambo, W. Li, Y.T. Zhao, C.L. Li, Porosity and its significance in plasma-sprayed coatings, Coatings 9 (7) (2019) 460, https://doi.org/10.3390/coatings9070460.
[29] F. Stolzenburg, J.D. Almer, K.N. Lee, B.J. Harder, K.T. Faber, Stresses in ytterbium silicate multilayer environmental barrier coatings, in: Proceedings of the Denver X-ray Conference (DXC 2011), 2011. Denver, CO.

[30] B.T. Richards, D. Zhu, L.J. Ghosn, H.N.G. Wadley, Mechanical properties of air plasma sprayed environmental barrier coating (EBC) materials, in: W.M. Kriven, J. Wang, D. Zhu, T. Fischer (Eds.), Developments in Strategic Ceramic Materials: A Collection of Papers Presented at, in: Proceedings of the 39th International Conference on Advanced Ceramics and Composites, John Wiley & Sons, Inc., Hoboken, 2015, pp. 219–237.
[31] B.T. Richards, Ytterbium Silicate Environmental barrier coatings, PhD Thesis, University of Virginia, 2015.
[32] J. Zamorano Igual, Q. Xu, Determination of the material constants of creep damage constitutive equations using Matlab optimization procedure, in: Proceedings of the 21st International Conference on Automation and Computing (ICAC), Glasgow, 2015, pp. 1–6, https://doi.org/10.1109/IConAC.2015.7313991.
[33] Y. Gong, C. Hyde, W. Sun, T. Hyde Determination of material properties in the Chaboche unified viscoplasticity model, Proc. Inst. Mech. Eng. Part L J. Mater. Des. Appl. 224 (1) (2010) 19–29, https://doi.org/10.1243/14644207JMDA273. ABR.
[34] X.F. Guo, A. Benaarbia, W. Sun, A. Becker, A. Morris, M. Pavier, P. Flewitt, M. Tierney, C. Wales, Optimisation and thermo-mechanical analysis of a coated steam dual pipe system for use in advanced ultra-supercritical power plant, Int. J. Press. Vessels Pip. 186 (2020) 104157, https://doi.org/10.1016/j.ijpvp.2020.104157.
[35] N. Rohbeck, P. Morrell, Pi Xiao, Degradation of ytterbium disilicate environmental barrier coatings in high temperature steam atmosphere, J. Eur. Ceram. Soc. 39 (2019) 3153–3163, https://doi.org/10.1016/j.jeurceramsoc.2019.04.034.
[36] B.T. Richards, K.A. Young, F. de Francqueville, S. Sehr, M.R. Begley, H.N. G. Wadley, Response of ytterbium disilicate–silicon environmental barrier coatings to thermal cycling in water vapor, Acta Mater. 106 (2016) 1–14, https://doi.org/10.1016/j.actamat.2015.12.053.
[37] J. Čadek, The back stress concept in power law creep of metals: a review, Mater. Sci. Eng. 94 (1987) 79–92, https://doi.org/10.1016/0025-5416(87)90324-7.
[38] Q. Long, C. Wu, T. Huang, X. Wang, A genetic algorithm for unconstrained multi-objective optimization, Swarm Evol. Comput. 22 (2015) 1–14, https://doi.org/10.1016/j.swevo.2015.01.002.
[39] J. Xu, V.K. Sarin, S. Dixit, S.N. Basu, Stability of interfaces in hybrid EBC/TBC coatings for Si-based ceramics in corrosive environments, Int. J. Refract. Met. Hard Mater. 49 (2015) 339–349, https://doi.org/10.1016/j.ijrmhm.2014.08.013.
[40] P. Kosky, R. Balmer, W. Keat, G. Wise, Exploring Engineering: An Introduction to Engineering and Design, 3rd ed., Elsevier Inc., 2013.
[41] D. Zhu, L.J. Ghosn, The development of environmental barrier coating systems for SiC-SiC ceramic matrix composites: environment effects on the creep and fatigue resistance, in: Proceedings of the Aerospace Coatings Conference & Exposition 2014: Development and Manufacturing Trend for the 21st Century Sheraton Bradley Hotel, Hartford, CT, USA, 2014. October 8.
[42] S.K. Mital, T.M. Ricks, S.M. Arnold, B.J. Harder, Modelling of the Influence of Thermally Grown Oxide (TGO) Layers on the Driving Forces in Environmental Barrier Coating Systems, National Aeronautics and Space Administration, 2021. Technical Report NASA/TM-20210014094.
[43] C.H. Cho, H.Y. Cha, H.K. Sung, Characterization of stiffness coefficients of silicon versus temperature using “Poisson’s Ratio” measurements”, J. Semicond. Technol. Sci. 16 (2016) 153–158, https://doi.org/10.5573/JSTS.2016.16.2.153.
[44] M.J. Ridley, K.Q. Tomko, J.A. Tomko, E.R. Hoglund, J.M. Howe, P.E. Hopkins, E. J. Opila, Tailoring thermal and chemical properties of a multi-component environmental barrier coating candidate (Sc0.2Nd0.2Er0.2Yb0.2Lu0.2)2Si2O7, Materialia 26 (2022) 101557, https://doi.org/10.1016/j.mtla.2022.101557.
[45] S.J. Zinkle, L.L Snead, Thermophysical and Mechanical Properties of SiC/SiC Composites, Oak Ridge National Lab, 1998, https://doi.org/10.2172/330618. Technical Report DOE/ER-0313/24.
[46] G Cibilakshmi, J. Jegan, A DOE approach to optimize the strength properties of concrete incorporated with different ratios of PVA fibre and nano-Fe2O3, Adv. Compos. Lett. 29 (2020) 1–16, https://doi.org/10.1177/2633366X20913882.
[47] V.K.R. Kodur, M.M.S. Dwaikat, Effect of high temperature creep on the fire response of restrained steel beams, Mater. Struct. 43 (2010) 1327–1341, https://doi.org/10.1617/s11527-010-9583-y.
[48] G. Canale, S. Andrews, F. Rubino, A. Maligno, R. Citarella, P.M. Weaver, Realistic stacking sequence optimisation of an aero-engine fan blade-like structure subjected to frequency, deformation and manufacturing constraints, Open Mech. Eng. J. 12 (2018) 151–163, https://doi.org/10.2174/1874155X01812010151.
[49] G. Canale, P.M. Weaver, F. Rubino, A. Maligno, R. Citarella, Lay-up optimization of laminated composites using a modified branch and bound method, Open Mech. Eng. J. 12 (2018) 138–150, https://doi.org/10.2174/1874155X01812010138.